Cancer Letters 455 (2019) 14–25

Contents lists available at ScienceDirect

Cancer Letters

journal homepage: www.elsevier.com/locate/canlet

Original Articles

FA-NBs-IR780: Novel multifunctional nanobubbles as molecule-targeted ultrasound contrast agents for accurate diagnosis and photothermal therapy of cancer

Yamei Shen[a,b,1], Wei Lv[a,1], Hengli Yang[a,d,1], Wenbin Cai[a], Ping Zhao[a], Li Zhang[a], Jian Zhang[c], Lijun Yuan[a,**], Yunyou Duan[a,*]

[a] Department of Ultrasound Medicine, Tang Du Hospital, Fourth Military Medical University, Xi'an, Shaanxi, 710038, China
[b] Department of Ultrasound Medicine, Shaanxi Provincial People's Hospital, Xi'an, Shaanxi, 710068, China
[c] Department of Biochemistry and Molecular Biology, Fourth Military Medical University, Xi'an, Shaanxi, 710023, China
[d] Department of Ultrasound Diagnosis, Air Force Characteristic Medical Center, Beijing, 100142, China

ARTICLE INFO

Keywords:
Molecule imaging
Nanobubbles
Ultrasonography
Near-infrared fluorescence
Photothermal therapy

ABSTRACT

Early accurate diagnosis and targeted therapy for cancer are essential to improve the prognosis of patients. With the emergence of molecular imaging, molecule-targeted ultrasound imaging for the non-invasive and precise detection of cancer has attracted increased attention. The investigation of molecule-targeted ultrasound contrast agents (UCAs) with excellent performance is urgently needed. In this study, we synthetized folic acid and IR-780 on self-made nanobubbles and prepared novel UCAs, named FA-NBs-IR780. The results showed that the conjugates had a uniform size distribution (591 ± 52 nm). *In vitro* and *in vivo* experiments demonstrated that FA-NBs-IR780 can target tumour cells via dual molecular targeting, perform enhanced-contrast ultrasound imaging and near-infrared fluorescence (NIRF) imaging for the precise detection of tumours, and induce targeted photothermal therapy in lesions irradiated at 808 nm. *Ex vivo* experiments further confirmed that FA-NBs-IR780 efficiently induced tumour cell apoptosis and inhibited tumour growth. The newly fabricated FA-NBs-IR780 were observed to be molecule-targeted dual-mode UCAs and may have potential applications in early accurate diagnosis and targeted therapy of cancer in the future.

1. Introduction

Currently, in cancer research, the accurate detection of early-stage cancer lesions is still a major issue. This detection is necessary to perform effective targeted treatment and improve the prognosis and survival rate of cancer patients [1]. Recently, molecule-targeted imaging has become a popular topic in preclinical research on cancer diagnostics and therapy. An increased amount of research has been carried out regarding the molecular imaging of cancer using X-ray radiography, computed tomography (CT), magnetic resonance imaging (MRI), and positron emission computed tomography (PECT), which are used to provide information for the precise targeting of cancer, to maximize anticancer efficacy, and to minimize treatment-related toxicity [2,3]. However, these imaging methods also have some disadvantages, such as radiation pollution, high costs, difficult to carry out routinely, and so on [4]. In recent years, ultrasound molecular imaging for cancer diagnosis and even treatment has attracted an increasing amount of attention due to its non-invasiveness, convenience, and cost effectiveness [5].

The use of appropriate ultrasound contrast agents (UCAs) is key for ultrasound molecular imaging. Traditional UCAs are produced as micro-bubbles (MBs) with diameters from 1 to 5 μm, which can only target molecular markers in the vasculature of tumours. The vascular endothelial gap of tumours is known to be approximately 380–780 nm, which is much wider than that of normal tissue [6]. Thus, tumour vasculature exhibits a passive targeting mechanism, called the contrast permeability and retention (EPR) effect [7–10]. However, the difficulty that MBs have in penetrating the vascular endothelial gaps of tumour limits their use in extra-vascular spaces. Accordingly, nanobubbles (NBs), i.e. nano-sized UCAs, have attracted a considerable amount of

* Corresponding author.
** Corresponding author.
E-mail addresses: yuanlj@fmmu.edu.cn (L. Yuan), duanyy@fmmu.edu.cn (Y. Duan).
[1] These authors contributed equally to this work.

https://doi.org/10.1016/j.canlet.2019.04.023
Received 28 January 2019; Received in revised form 30 March 2019; Accepted 17 April 2019

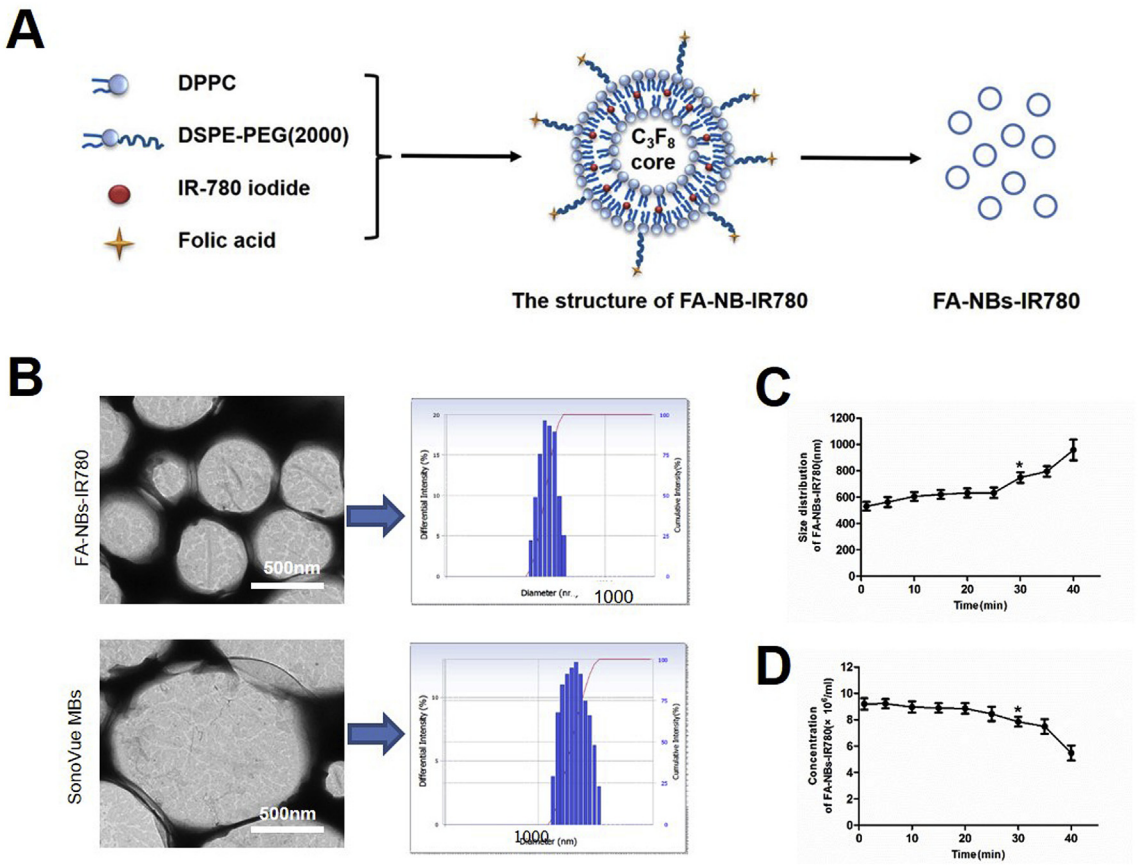

Fig. 1. Preparation and characterization of FA-NBs-IR780. (A) Schematic illustration the structure of FA-NBs-IR780. (B) Comparison of FA-NBs-IR780 and SonoVue MBs in TEM imaging and size distribution. (C and D) Changes of FA-NBs-IR780 size distribution and concentration for 40 min $*$ $p < 0.05$: significantly different compared to the values recorded at 1 min.

attention [11]. NBs are advantageous for the ultrasound imaging of tumours mainly due to their unique size and selective accumulation in the tumour interstitial space via the EPR effect, allowing for the molecular imaging and treatment of tumours. However, NBs lack tumour target markers and can thus be easily cleared by the reticuloendothelial system (RES) in the liver and spleen, resulting in low target efficacy [12,13]. One of the methods used to resolve this problem is by the linking of special ligands on the NBs to increase their adherence to cancer cells. In a previous work, we successfully synthesized the "NBs–Affibody" to target the human epidermal growth factor receptor 2(HER2) molecule to carry out ultrasound molecule-targeted imaging of breast cancer *in vivo* [13].

The folate receptor (FR), which is known to be overexpressed in several human cancers, including lung, breast, ovarian, endometrium, kidney, colon, and brain cancer, but is rare in healthy tissues, has attracted considerable research attention [14–18]. To date, a number of folic acid (FA)-conjugated imaging and therapeutic agents have been evaluated in preclinical studies, including UCAs and nanoparticle agents [19,20]. In addition, IR-780 iodide, a near-infrared fluorescence (NIRF) dye, is a lipophilic, cationic heptamethine dye with high fluorescence intensity, which preferentially accumulates in tumours, resulting in targeted tumour imaging [21,22]. Moreover, the IR-780 iodide can also be used as a photoactive material for cancer therapy due to its photothermal therapy (PTT) effects, absorbing light at local sites and inducing heat [23–25]. Despite its potential, the clinical application of IR-780 iodide has been restricted due to its poor aqueous solubility, as well as a result of only a small amount of it being able to reach tumours via the blood. Moreover, an increased dose of IR-780 iodide also increases toxicity.

In this study, we fabricated multifunctional nanobubbles, FA-NBs-IR780, which combined the targeting advantage of FA and IR-780 iodide and the photothermal effects of IR-780 iodide. The results indicated that FA-NBs-IR780 could efficiently detect lesions via dual-mode imaging and induce robust therapeutic effects when combined with laser treatment. These findings suggest that FA-NBs-IR780 could serve as promising molecular imaging and therapy agents for cancer.

2. Materials and methods

2.1. Materials

The lipid components of nanobubbles, including 1,2-dipalmitoyl-sn-glycero-3-phosphocholine (DPPC), 1,2-distearoyl-sn-glycero-3-phosphoethanolamine-N- [(polyethylene glycol)-2000] [DSPE-PEG (2000)], DSPE-PEG (2000)-FA, and DSPE-PEG (2000)-FITC were purchased from Avanti Polar Lipids Inc. (Alabaster, AL, USA). The core of the nanobubbles, octafluoropropane (C_3F_8), was purchased from the R&D Centre for Specialty Gases at the Research Institute of Physical and Chemical Engineering of the Nuclear Industry (Beijing, China). The heptamethine indocyanine dye IR-780 iodide was purchased from Sigma Aldrich (St. Louis, MO, USA).

2.2. Synthesis of FA-NBs-IR780

The FA-NBs-IR780 were prepared using the thin-film hydration and mechanical vibration method, as previously described by our laboratory [12,13]. Briefly, DPPC, DSPE-PEG (2000)–FA, and IR-780 iodide solution (1 mg/mL in chloroform) were mixed together in a quality ratio of 10:4:0.3. Then, the lipid mixture was dissolved in 2 mL of chloroform. The mixture was removed to a 25-mL glass flask with a

rotavapor. Rotary evaporation was performed for 10 min at 55 °C and 130 rpm in a commercially available rotary evaporator (New Brunswick Scientific, New Brunswick, NJ, USA) to generate a dried thin-lipid film. The dried phospholipid blends were hydrated in 1.5 mL of hydration liquid (10% glycerol and 90% 1 × PBS, *v/v*). Then, the flask was placed in an incubator-shaker (New Brunswick Scientific, New Brunswick, NJ, USA) at 37 °C and 120 rpm for 60 min to prepare a liposomal film suspension. Subsequently, the liposomal suspension was placed in vials sealed with rubber caps. The gas in the vials was withdrawn using a 50-mL syringe with a long needle, followed by the addition of C_3F_8 gas (which will later form the bubble cores) to the vials, until the pressure in the vial was equalized. Finally, the vials were placed in a mechanical shaker (Ag and Hg mixer, Xi'an, China) and shaken by mechanical vibration for 90 s (Fig. 1A). The parent suspensions of FA-NBs-IR780 were immediately placed on ice. The whole procedure was carried out in the absence of light.

NBs, FA-NBs, and NBs-IR780 were also included as controls, wherein the synthesis process was as described above. The fluorescent dye FITC was additionally incorporated into the liposome shell for the optical detection of NBs by confocal laser scanning microscopy (CLSM) and flow cytometry. Before examination, NBs, FA-NBs, NBs-IR780, and FA-NBs-IR780 were diluted with 1 × PBS (phosphate buffer solution, pH 7.4) to the same concentration (6×10^6 bubbles/mL), which were counted using a haemocytometer.

2.3. Characterization of FA-NBs-IR780

The encapsulation efficiency (EE) and drug loading (DL) of IR-780 in FA-NBs-IR780 were measured using a UV–vis spectrophotometer (Mapada UV-6100S, Shanghai, China) (Supplementary methods). The particle size and polydispersity index (P.I.) of the FA-NBs-IR780 were assessed using a nanometre particle size/zeta potential analyser (NanoPlus 300, Beckman Coulter, Inc., USA) at room temperature. To observe more clearly, one drop of diluted FA-NBs-IR780 was placed onto a copper grid covered with amorphous carbon and dried for 30 min. After evaporation, the morphology and size of the FA-NBs-IR780 were assessed via transmission electron microscopy (TEM, T12 Tecnai G2, FEI Company, USA). Commercially-available SonoVue MBs were used as the control. The size distribution and concentration of FA-NBs-IR780 were measured for 40 min to evaluate the stability of FA-NB-IR780. Briefly, a parent suspension of FA-NBs-IR780 was diluted ten-fold with 1 × PBS at 37 °C. The nanometre particle size/zeta analyser was used to measure the size distribution of FA-NB-IR780 and a haemocytometer was used to calculate the number of FA-NB-IR780 at 5-min intervals. All the experiments were carried out in triplicate.

2.4. Echogenicity and NIRF imaging of FA-NBs-IR780 in vitro

To evaluate the echogenicity of FA-NBs-IR780, the FA-NBs-IR780 and control SonoVue MBs were diluted with 1 × PBS to a final concentration of 6.0×10^6 bubbles/mL. About 500 μL of either 1 × PBS, diluted FA-NBs-IR780, or control SonoVue MBs were added to a check model made from a latex glove fingertip, maintained in a water bath containing 10 mL 1 × PBS. A clinical ultrasound system (Esaote, MyLab Twice) was used with a LA523 high-frequency linear transducer. The ultrasound-contrast process was selected with a centre frequency of 7.5 MHz and a mechanical index (MI) of 0.08. All the images were recorded as dynamic imaging files. Image analysis was performed using Image-Pro Plus software, version 6.0.

The NIRF optical characteristics of FA-NBs-IR780 were assessed using CLSM (Nikon A1R, Japan) at room temperature. Briefly, one drop of diluted FA-NBs-IR780 was placed between glass slides and was observed using CLSM, with an excitation wavelength of 640 nm and an emission wavelength of 700–800 nm.

2.5. Cell culture

The human glioblastoma cell line U87 and the human breast cancer cell line MDA-MB-231 (Chinese Academy of Sciences Cell Bank, Shanghai, China), both of which over-express FR, were used. Dulbecco's modified Eagle's medium (DMEM) supplemented with foetal bovine serum (FBS, 10%) and penicillin/streptomycin (1%) was used as the cell culture medium. Cells were cultured in a humidified atmosphere at 37 °C in a 5% CO_2 incubator; the medium was changed every two days. Before the experiments, the cells were pre-cultured until 70–80% confluence was reached.

2.6. In vitro affinity analysis of FA-NBs-IR780 to cancer cells

The U87 and MDA-MB-231 cell lines were used to analyse cancer cell targeting specificity using CLSM and flow cytometry. Briefly, FITC-labelled NBs, FITC-labelled FA-NBs, FITC-labelled FA-NBs-IR780, and NBs-IR780 were diluted to a final concentration of 6.0×10^6 bubbles/mL. Free IR-780 iodide was dissolved in dimethylsulfoxide (DMSO, 0.2 mg/mL), to a final concentration was 20 μg/mL. For the CLSM studies, the U87 and MDA-MB-231 cells were seeded into ten 15-mm glass-bottom dishes (2.5×10^5 cells per dish) and cultured overnight. Then, the culture medium was charged with FA-NBs-IR780 (FITC), NBs-IR780, FA-NBs (FITC), NBs (FITC), and free IR-780 (100 μL per dish), respectively. After a 40-min incubation period, the cells were fixed and washed three times with 1 × PBS, followed by staining with Hoechst 33342 (10 μg/mL, 1 mL per dish). After incubation for 15 min in 37 °C, the dishes were washed thrice with PBS. The fluorescence signals were observed by CLSM. The excitation and emission wavelengths of IR-780 iodide were 640 nm and 700–800 nm, respectively. The excitation and emission wavelengths of FITC were 488 nm and 525 nm, respectively.

Flow cytometry was used to quantitatively evaluate the cancer cellular target efficiency further. U87 cells were seeded into six-well culture plates (5×10^5 cells per well) and incubated overnight. Then, the medium was replaced with FA-NBs-IR780 (FITC), NBs-IR780, FA-NBs (FITC), NBs (FITC), and free IR-780 (100 μL per well), respectively. After a 40-min incubation period, the cells were washed with cold PBS. Finally, the cells were detached, transferred to a sterile test tube (1.0×10^6 cells/mL), and measured using a flow cytometer assay (FC500 MCL, Beckman Coulter, Inc., USA). All the experiments were performed in the absence of light and in triplicate.

2.7. In vitro analysis of the photothermal efficiency of FA-NBs-IR780 upon near-infrared (NIR) irradiation

To evaluate the photothermal efficiency of FA-NBs-IR780 upon NIR irradiation, we monitored the temperature changes under NIR irradiation and evaluated the photothermal efficiency by CLSM and CCK-8 *in vitro*. First, U87 cells were seeded onto five 15-mm glass-bottom dishes at 2.5×10^5 cells per dish and cultured overnight. FA-NBs-IR780 and the controls NBs, FA-NBs, NBs-IR780, and free IR-780 iodide at a concentration of 20 μg/mL, were added to the dishes (100 μL per dish). After 40 min of incubation, the cells were extensively washed with 1 × PBS and fresh medium was added. This was followed by 808 nm laser irradiation with a power density of 1 W/cm^2 for 2 min. Meanwhile, the temperature of the dish was measured over 5 min using an IR thermometer (Unitrend UT 300S, Guangdong, China). After treatment, the cells were stained with 5 μg/mL, 100 μL per dish, of propidium iodide (PI) (Invitrogen, Grand Island, NY) for 15 min at room temperature to label the necrotic and late apoptotic cells. Finally, the cells were observed by CLSM. The excitation and emission wavelengths were 543.5 nm and 600–680 nm, respectively. The photothermal efficiency was also quantitatively evaluated using a CCK-8 assay. First, the U87 cells were seeded onto 96-well plates (1×10^4 cells per well), where each group had 6 sub-wells. The cells were incubated overnight and treated as above. At the end of the experiments, the cell viability

was evaluated by CCK-8 and expressed as the percentage of surviving cells compared to the untreated group. All the experiments were carried out in triplicate.

2.8. Mouse xenograft model

Female BALB/c nude mice (4–6 weeks old and weighing 18–20 g) were purchased from Vital River Laboratory Animal Technology Co., Ltd. (Beijing, China). All the animals received care in compliance with the guidelines of the Guide for the Care and Use of Laboratory Animals by the National Institutes of Health. All the procedures were approved by the Institutional Animal Care and Use Committee of the Fourth Military Medical University. To establish the mouse xenograft model, U87 cells (5×10^6 cells) were suspended in 200 μL growth of medium and injected subcutaneously into the right flank of the mice. All *in vivo* experiments were initiated when the tumour volumes reached 100–150 mm^3.

2.9. Ultrasound-enhanced imaging and NIRF imaging of the xenograft

For ultrasound-enhanced imaging, tumour-bearing mice (n = 25) were randomly separated into five groups, each receiving either SonoVue MBs, NBs, FA-NBs, NBs-IR780, or FA-NBs-IR780 via injection, respectively (n = 5 for each group). The contrast agents were diluted with PBS to the same concentration (6×10^6 bubbles/mL) and sterilized by Co-60 irradiation for 30 min before being injected via the tail vein (200 μL per mouse). The tumour-bearing mice were fixed on a flat platform and anesthetized via an intraperitoneal injection of 1% sodium pentobarbital/100 μL. The Esaote MyLab Twice ultrasound system together with a LA523 high-frequency linear transducer was used, with the centre frequency of 7.5 MHz and MI of 0.08 to prevent the destruction of the NBs. The ultrasound probe was placed gently at the top of the tumour, which was covered with 5 mm thick commercial diagnostic ultrasound gel. First, the 2D ultrasound imaging and colour doppler flow imaging (CDFI) of tumours was performed. Then, the contrast agent distribution was monitored for more than 300 s from the time of injection. In this experiment, all the parameters were recorded by dynamic memory. The regions of interest (ROIs) for tumour imaging were determined using the contrast agent margin. Image analysis was performed using the Image-Pro Plus software program (version 6).

The NIRF imaging of tumour-bearing mice was visualized using an *in vivo* fluorescence imaging system (IVIS, Lumina II, Caliper, Boston, MA, USA). The fluorescent dye FITC was additionally incorporated into the liposome shell for the optical detection of NBs by IVIS system. At 24 h post-injection, the mice were administered inhalation anaesthesia with isopropyl fluoride and were observed via the IVIS system. IR-780 iodide was observed with an emission wavelength at 745 nm and ICG reception. The excitation and emission wavelengths of FITC were 488 nm and 525 nm, respectively. The fluorescence image intensity was analysed using the IVIS Lumina II system.

2.10. Bio-distribution of FA-NBs-IR780

To observe the bio-distribution of FA-NBs-IR780, fifteen tumour-bearing mice were injected with diluted FA-NBs-IR780 (200 μL per mouse). Then the mice were randomly chosen to be sacrificed at 3 min, 3 h, 12 h, 24 h, and 48 h post-injection (n = 3 for each time point). The organs, including the heart, liver, spleen, lungs, and kidneys, and the tumour were harvested for bio-distribution imaging and quantitative analysis using the IVIS Lumina II system.

2.11. In vivo analysis of the antitumor effects of FA-NBs-IR780 upon NIR irradiation

The U87 tumour-bearing mice (n = 25) were used to observe the antitumor ability of FA-NBs-IR780 upon NIR irradiation. Before injection, the contrast agents were sterilized by Co-60. The mice were randomly given 200 μL FA-NBs-IR780, NBs-IR780, FA-NBs, saline treatment, or 50 μL free IR-780 iodide (0.2 mg/mL) (n = 5 per group). Then, 12 h post-injection, the tumours were exposed to 808 nm laser irradiation at a power density of 1 W/cm^2 for 2 min. The temperatures at the tumour site were recorded immediately after NIR irradiation using an IR thermometer. The tumour volumes were measured using 2D ultrasound and were calculated using the following formula: tumour volume = length × width × height × $6/\pi$. Throughout the experiments, the tumour volumes and body weights were measured every 3 days. The morphology and surface changes of the tumours were photographed using a digital camera every 3 days. Comparative tumour volumes were calculated as V/V_0, where V_0 denotes the original tumour volume before treatment.

The antitumor efficacy of FA-NBs-IR780 upon NIR irradiation was further evaluated by immunohistochemical analyses. Three days after treatment, 10 cancer-bearing mice (2 mice from each group) were sacrificed, and the tumours were harvested. The tumours were washed with PBS, fixed in 4% formaldehyde, and embedded in paraffin [26]. The terminal deoxynucleotidyl transferase dUTP nick end labelling (TUNEL staining) was used to evaluate cell apoptosis, and proliferating cell nuclear antigen (PCNA) immunolocalization was used to evaluate cell proliferation. The apoptosis index (AI) and proliferation index (PI) were calculated as percentages of positively stained cells for all cells from six randomly chosen fields at 200× magnification, then analysed using Image-Pro Plus software (version 6.0).

2.12. Statistical analysis

All the data are presented as the mean ± SD (standard deviation). Statistical analysis of the data was performed using the Student's *t*-test and one-way ANOVA with GraphPad Prism (version 5.0) (GraphPad, San Diego, CA). Statistical significance of variational trends at multiple time points was performed using repeated-measures ANOVA. Pairwise comparisons between experimental groups at a single point of time were analysed using the least statistical significance (LSD) *t*-test (SPSS 19.0 software). $p < 0.05$ was considered statistically significant.

3. Results

3.1. Preparation and characterization of FA-NBs-IR780

The FA-NBs-IR780 were successfully synthesized by the thin-film hydration and mechanical vibration method (Fig. 1A). The EE of IR-780 in FA-NBs-IR780 was 60.18 ± 8.56%, and the DL was 1.31 ± 0.28% via a UV–vis spectrophotometer (Supplementary Fig. S1). The TEM images revealed that the FA-NBs-IR780 were approximately spherical in morphology and were well-dispersed in the solution, with a small size of approximately 500 nm. The size of the SonoVue MBs was 1–2 μm, much larger than the FA-NBs-IR780 (Fig. 1B). Size distribution analysis further showed that the average diameter of the FA-NBs-IR780 was 591 ± 52 nm, while the average diameter of the SonoVue MBs was 1575 ± 63 nm (Fig. 1B, $p < 0.01$: significantly different compared to FA-NBs-IR780). The P.I. of the FA-NBs-IR780 was 0.313 ± 0.061, and the P.I. of the SonoVue MBs was 0.286 ± 0.052 ($p > 0.05$: compared to FA-NBs-IR780). The low P.I. value indicated a high homogeneity in the size of the NBs. These results confirmed that the FA-NBs-IR780 formed by self-assembly are spherical and are nano-sized. As shown in Fig. 1C and D, the size distribution of FA-NB-IR780 was not significantly changed within 25 min compared to that at 1 min (632.8 ± 40.6 nm vs. 530.2 ± 32.9 nm, $p > 0.05$). Nevertheless, it increased at 30 min (749.2 ± 40.3 nm at 30 min vs. 530.2 ± 32.9 nm at 1 min, $p < 0.05$). Similarly, the concentration of FA-NB-IR780 was stable within 25 min compared to that at 1 min ($8.45 \pm 0.54 \times 10^6$/mL vs. $9.21 \pm 0.43 \times 10^6$/mL, $p > 0.05$), but was significantly decreased at 30 min ($7.86 \pm 0.38 \times 10^6$/mL at

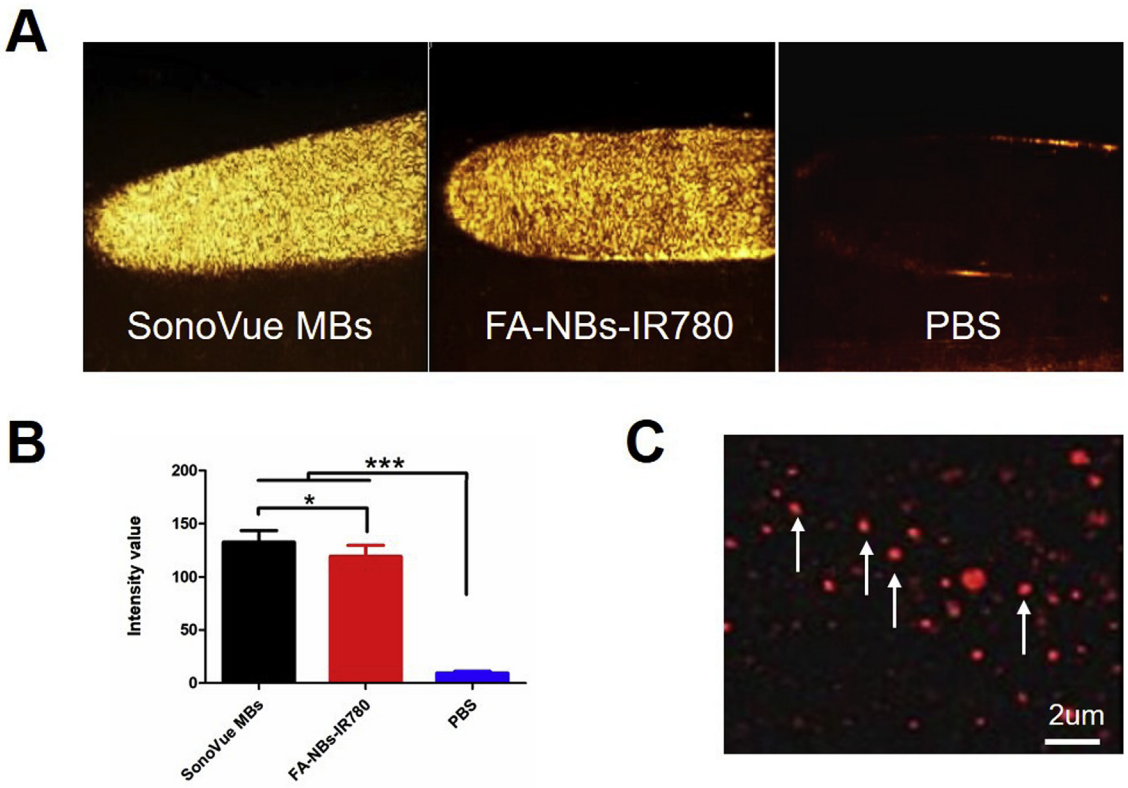

Fig. 2. Echogenicity and NIRF imaging capacity of FA-NBs-IR780 *in vitro*. (A) Ultrasound contrast-enhanced imaging of SonoVue MBs, FA-NBs-IR780, and PBS at 7.5 MHz *in vitro*. (B) Statistics of intensity value with ultrasound contrast-enhanced imaging. $* p < 0.05$: significantly different compared to SonoVue MBs; $*** p < 0.001$: significantly different compared to PBS. (C) NIRF imaging of FA-NBs-IR780 observed by CLSM. The white arrow points to FA-NBs-IR780.

30 min vs. 9.21 ± 0.43 × 10^6/mL at 1 min, $p < 0.05$). These results indicate that the FA-NB-IR780 were relatively stable within 25 min.

3.2. Echogenicity and NIR imaging capacity of FA-NBs-IR780 in vitro

In the following experiments, the echogenicity of FA-NBs-IR780 was analysed by *in vitro* ultrasound contrast imaging. As expected, the echogenicity of FA-NBs-IR780 and SonoVue MBs all presented bright enhanced imaging (Fig. 2A). Compared to PBS, the intensity values of the ultrasound contrast imaging of FA-NBs-IR780 were significantly higher (119.21 ± 3.05 vs. 9.34 ± 0.35, $p < 0.001$) (Fig. 2B). The intensity values of FA-NBs-IR780 were slightly lower compared to those of SonoVue MBs (119.21 ± 3.05 vs. 132.72 ± 2.11, $p < 0.05$) (Fig. 2B), possibly because the small size resulted in low backscattering [27]. However, the intensity of the contrast imaging was sufficient for *in vivo* imaging applications. These results confirmed that the FA-NBs-IR780 could potentially be used as UCAs for *in vivo* applications.

Then, we examined the NIRF imaging capacity of FA-NBs-IR780 under CLSM. As expected, FA-NBs-IR780 showed red dots smaller than 1 μm (Fig. 2C), which not only proved that IR-780 iodide was encapsulated in NBs successfully, but also indicated that FA-NBs-IR780 could be visualized by NIR optical imaging.

3.3. In vitro cancer targeting efficiency of FA-NBs-IR780

The U87 and MDA-MB-231 cells were used to test the cancer targeting efficiency of FA-NBs-IR780. As observed by CLSM, cells treated with NBs (FITC) presented no fluorescence. There was a slight red fluorescence observed in the cells treated with free IR-780 and a greater amount of red fluorescence in cells treated with NBs-IR780. Cells treated with FA-NBs (FITC) presented a greater amount of green fluorescence. Notably, cells treated with FA-NBs-IR780 (FITC) presented significantly strong green and red fluorescence, indicating that more NBs were associated with cancer cells (Fig. 3A).

The flow cytometry results were in accordance with CLSM. As shown in Fig. 3B, the associative property of NBs (FITC) and cancer cells was 0.5%. Moreover, a very low cancer targeting binding rate (1.9 ± 0.5%) was observed between free IR-780 and cancer cells. A higher corresponding cancer target rate was observed in the FA-NBs (FITC) group (16.6 ± 2.8%) and NBs-IR780 group (27.6 ± 3.9%). The FA-NBs-IR780 adhered more to cancer cells with a significantly higher target binding rate of 98.3 ± 3.7%.

3.4. In vitro the photothermal efficiency of FA-NBs-IR780 upon NIR irradiation

FA-NBs-IR780 are expected have an antitumor ability when exposed to NIR irradiation due to the PTT effects. The temperature profile revealed that the temperature of NBs, FA-NBs, free IR-780, NBs-IR780, and FA-NBs-IR780 groups maximally increased to 27, 28, 31, 39, and 45 °C upon NIR irradiation (Supplementary Fig. S2). The maximum temperature of FA-NBs-IR780 increased by 20 °C, while the negative control blank NBs did not experience a significant temperature increase. The results of CLSM and CCK-8 showed that no fluorescence was observed in cells treated with blank NBs or FA-NBs upon NIR irradiation, and a high cell viability (94.14 ± 4.62% and 87.37 ± 3.26%) was obtained. However, the viability of U87 cells slightly decreased (64.62 ± 5.97%) and displayed some red fluorescence signals when the cells were treated with free IR-780 upon NIR irradiation (Fig. 4A and B). Moreover, NBs-IR780 showed stronger cancer cellular cytotoxicity when combined with NIR irradiation. As shown in Fig. 4, a greater amount of red fluorescence signals and a lower cell viability (53.17 ± 6.49%) were observed. Strikingly, most of the U87 cells treated with FA-NBs-IR780 were found to be dead upon NIR irradiation.

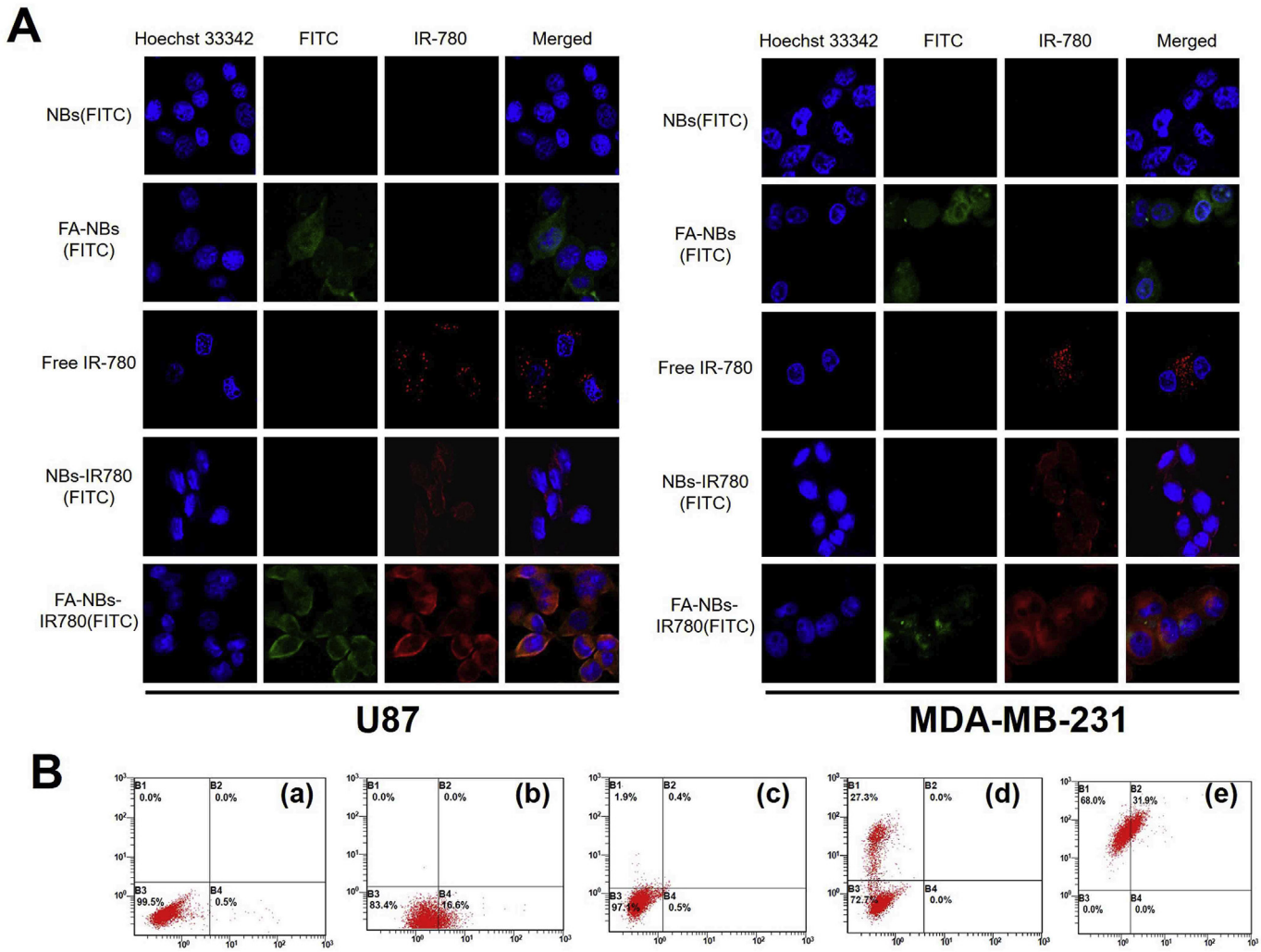

Fig. 3. Cancer cellular targeting ability of FA-NBs-IR780 via CLSM and flow cytometry *in vitro*. (A) The cancer cellular targeting ability of contrast agents in U87 cells and MDA-MB-231 cells via CLSM. Blue, nuclei labelled with Hoechst 33342; green, labelled with FITC; red, labelled with IR-780 iodide. Scale bar: 20 μm. (B) The cancer cellular targeting ability of contrast agents in U87 cells via flow cytometry. (a) U87 cells incubated with NBs (FITC); (b) U87 cells incubated with FA-NBs (FITC); (c) U87 cells incubated with free IR-780; (d) U87 cells incubated with NBs-IR780; (e) U87 cells incubated with FA-NBs-IR780(FITC). Results from flow cytometry analysis in each quadrant (B) are labelled as follows: (B1) IR-780 positive, FITC negative. (B2) cells positive for both IR-780 and FITC. (B3) cells negative for both IR-780 and FITC. (B4) IR-780 negative, FITC positive. (For interpretation of the references to colour in this figure legend, the reader is referred to the Web version of this article.)

The cell viability was very low (16.64 ± 2.51%), with significant differences compared to the other groups (Fig. 4A and B). Thus, FA-NBs-IR780 upon NIR irradiation exhibited superior phototherapy efficacy of cancer cells *in vitro*.

3.5. Ultrasound-enhanced imaging and NIRF imaging of FA-NBs-IR780 in vivo

To test whether the xenograft could be efficiently imaged by FA-NBs-IR780, tumour-bearing mice were injected with FA-NBs-IR780, while the SonoVue MBs, NBs, NBs-IR780, and FA-NBs were included as a control. As shown in Fig. 5C, statistical differences were observed in the imaging intensity of the different groups. At 10 s, the imaging intensity of the SonoVue MBs was greater than that of the NBs; however, these differences were not statistically significant. Then the imaging intensity of the SonoVue MBs decreased gradually. The imaging intensity of blank NBs was increased over the first 30 s and then decreased quickly with time. The imaging intensity of NBs-IR780 and FA-NBs decreased slower than the NBs after 30 s. Notably, at 30 s, the ultrasound peak intensity of FA-NBs-IR780 was the highest and higher than that of NBs at the peak intensity ($p < 0.05$). The duration time of FA-NBs-IR780 was the longest, the imaging intensity even higher than SonoVue MBs and NBs at 300 s ($p < 0.05$).

To further explore whether FA-NBs-IR780 could target tumour site and be used for optical imaging, the mice were imaged by IVIS system. As shown in Fig. 6, no fluorescence signal of blank NBs was observed at the tumour sites. Weak fluorescence signals were exhibited at the tumour sites of mice treated with NBs-IR780 and FA-NBs, which indicated that they accumulated only to a small degree at tumour sites. Notably, a much brighter fluorescence was observed at the tumour site in the mice receiving FA-NBs-IR780, with a higher radio-efficiency than that of NBs-IR780 and FA-NBs ($p < 0.05$), suggesting that FA-NBs-IR780 accumulated massively at tumour sites and could also be suitable for optical imaging of cancer *in vivo* (Fig. 6B).

3.6. Bio-distribution of FA-NBs-IR780 in vivo

For a more accurate measurement, the bio-distribution of FA-NBs-IR780 over a series of time intervals was visualized using the IVIS system. As shown in Fig. 7A and B, the fluorescence imaging of the

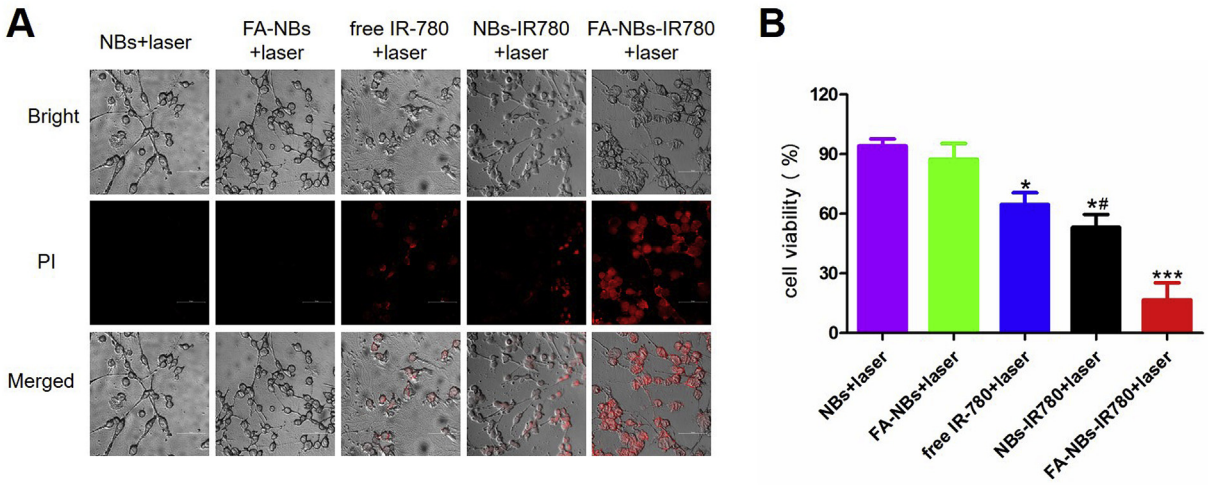

Fig. 4. Photothermal efficiency of FA-NBs-IR780 upon NIR irradiation using U87 cells *in vitro*. (A) CLSM images of U87 cells treated with NBs + laser, FA-NBs + laser, free IR-780 + laser, NBs-IR780 + laser, and FA-NBs-IR780 + laser, respectively. PI was used to stain the nuclei of the dead cells (red). (B) CCK-8 appraisal of cell viability after PTT treatment *in vitro*. $*p < 0.05$: significantly different compared to the FA-NBs + laser group and NBs + laser group; $^{\#}p < 0.05$: significantly different compared to the free IR-780 + laser group; $***p < 0.001$: significantly different compared to the NBs-IR780 + laser group. (For interpretation of the references to colour in this figure legend, the reader is referred to the Web version of this article.)

heart and spleen was only observed in the first 3 min. The fluorescence imaging intensity of the liver, kidneys, and lungs had the same variation trends. They all presented a decreasing tendency after reaching peak intensity at 3 min. The fluorescence imaging of the kidneys and liver disappeared within 12 h and 48 h, respectively. A bright fluorescence signal was found in the lungs, which, due to C_3F_8, was mainly metabolized by the lungs. Notably, the fluorescence imaging intensity of the tumour also appeared 3 min after tail veil injection but increased with time, attaining a peak intensity at 12 h, which was significantly higher than the intensity of the tumour at 3 h or 24 h ($p < 0.05$) (Fig. 7C). These results also indicate that the optimal PTT therapy time is 12 h post-injection.

3.7. Antitumor efficacy of FA-NBs-IR780 upon NIR irradiation in vivo

After confirming the preferential accumulation of FA-NBs-IR780 at the tumour site and the photothermal activity of IR-780, we investigated whether the nanobubbles could promote tumour apoptosis upon NIR irradiation. As the results showed, there was no obvious increase in the surface temperature of the tumours in the control group or the FA-NBs group upon NIR irradiation. The temperature did increase, from 33 °C to 37 °C, in the free IR-780 and NBs-IR780 groups. Notably, the tumour surface temperature of the FA-NBs-IR780 group upon NIR irradiation rapidly increased from 33.4 °C to 44.4 °C under the same irradiation conditions. The maximum temperature was 46.9 °C (Fig. 8A).

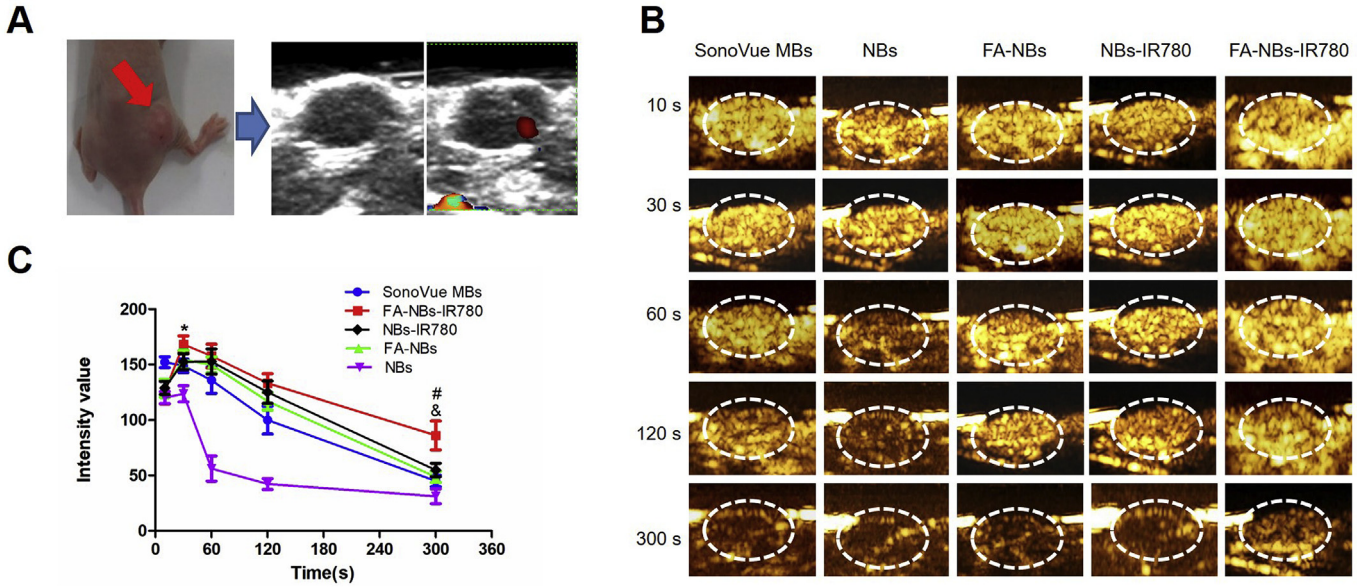

Fig. 5. Ultrasound contrast-enhanced imaging of FA-NBs-IR780 using U87 xenografts in nude mice. (A) U87 xenograft in nude mouse model (red arrow), 2D ultrasound images and CDFI of xenografts. (B) Ultrasound contrast-enhanced imaging of xenografts after injected SonoVue MBs, NBs, FA-NBs, NBs-IR780, and FA-NBs-IR780 at various time points. (C) Corresponding time-intensity curves of SonoVue MBs, NBs, FA-NBs, NBs-IR780, and FA-NBs-IR780 with data extracted from (B). $*p < 0.05$: significantly different compared to ultrasound contrast-enhanced intensity of NBs at the peak intensity time; $^{\&}$ and $^{\#}p < 0.05$: significantly different compared to ultrasound contrast-enhanced intensity of SonoVue MBs and NBs at 300 s, respectively. (For interpretation of the references to colour in this figure legend, the reader is referred to the Web version of this article.)

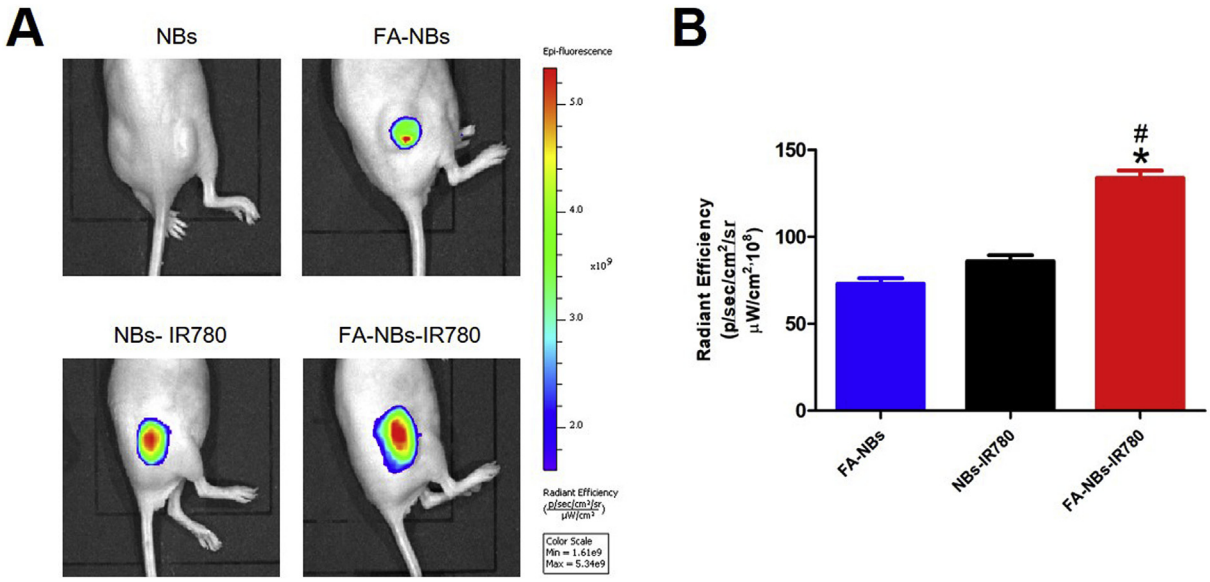

Fig. 6. NIRF imaging of FA-NBs-IR780 using U87 xenografts in nude mice. (A) NIRF imaging of tumour-bearing mice intravenously injected with NBs, FA-NBs, NBs-IR780, and FA-NBs-IR780 *in vivo*. (B) Fluorescence intensity of FA-NBs, NBs-IR780, and FA-NBs-IR780 with data extracted from (A). * and $^{\#}p < 0.05$: significantly different compared to the fluorescence intensity of FA-NBs and NBs-IR780 at 24 h post-injection, respectively.

As shown in Fig. 8, the control group and the FA-NBs group showed a progressive increase in tumour volume after PTT treatment. The relative tumour volume (V/V_0) ranged from 1 to 6.886 ± 0.745 and 6.537 ± 0.936 at 15 days; and no significant changes of the tumour surface were observed. There were also no significant changes of the tumour surface in the free IR-780 group after PTT treatment. The V/V_0 of the tumour in free IR-780 group was lower than that of the tumours in the control group and the FA-NBs group at 15 days (4.385 ± 0.642 vs. 6.886 ± 0.745 and 6.537 ± 0.936, $p < 0.05$). The NBs-IR780 group showed a small scab on the tumour surface after PTT treatment, and the growth rate was slower. The V/V_0 of the tumour in the NBs-IR780 group was lower than that of the tumour in the free IR-780 group at 15 days (3.535 ± 0.779 vs. 4.385 ± 0.642, $p < 0.05$). It should be noted that the tumour volume was over three-fold the original size at 15 days. However, the growth of the tumour was significantly inhibited in the FA-NBs-IR780 group. The tumour surface turned black and scabbed at 3 days. Subsequently, the tumour disappeared at 15 days (Fig. 8B). The volume was found to decrease strikingly (V/V_0 from 1 to 0.156 ± 0.012 at 15 days, Fig. 8D), at a statistically significant rate compared to the other groups ($p < 0.01$). Body weight loss was considered an indicator of treatment-induced toxicity [22]. Neither was there any significant decrease in body weight found in the mice treated with FA-NBs-IR780 upon laser irradiation, nor were there any significant changes in body weight observed between the groups (Fig. 8E),

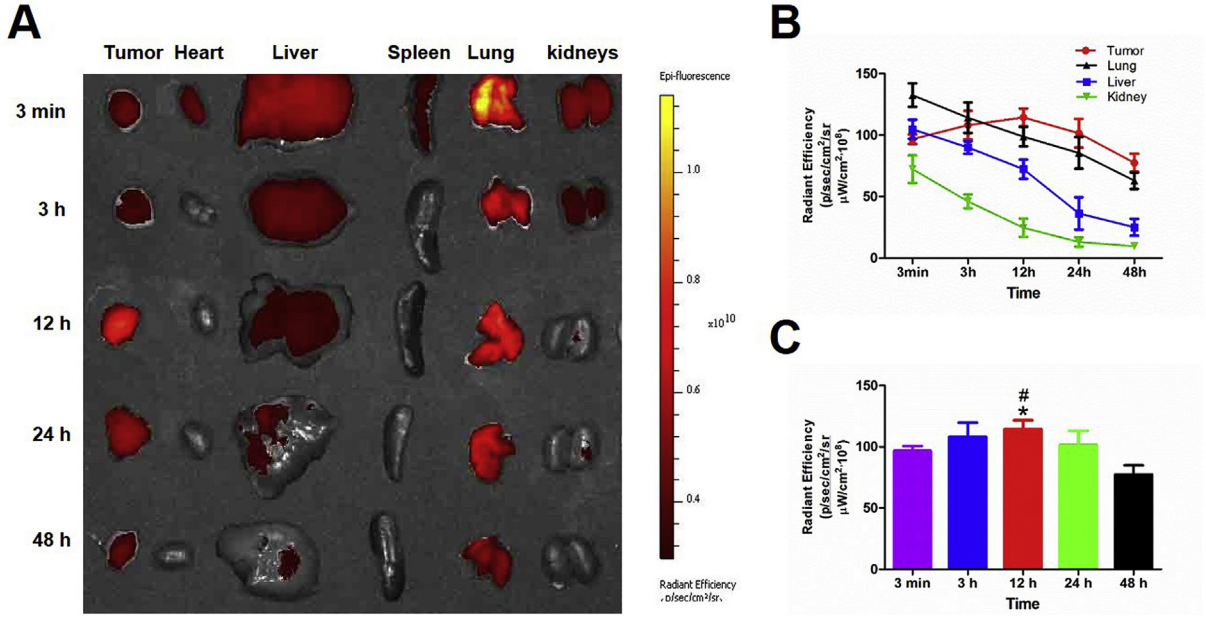

Fig. 7. *Ex vivo* fluorescence imaging of tumour-bearing mice injected with FA-NBs-IR780 at different time intervals. (A) *Ex vivo* fluorescence imaging of the heart, liver, spleen, lungs, kidneys, and tumour, respectively. (B) ROI analysis of organs excised from tumour-bearing mice treated with FA-NBs-IR780 by *ex vivo* fluorescence imaging for different time intervals. (C) ROI analysis the fluorescence imaging of tumours treated with FA-NBs-IR780 for different time intervals. * and $^{\#}p < 0.05$: significantly different compared to the fluorescence intensity of the tumours at 3 h and 24 h, respectively.

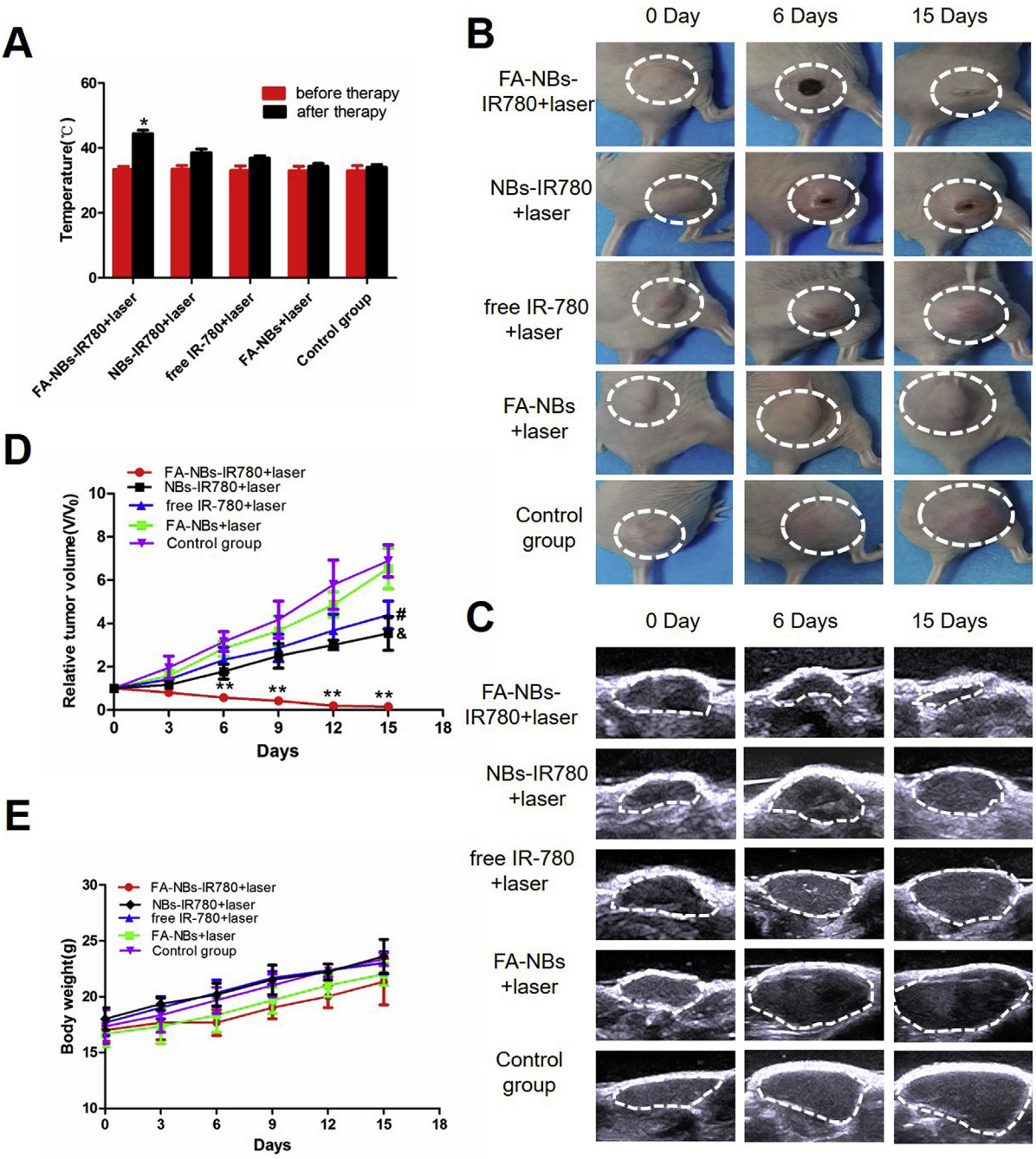

Fig. 8. Antitumor efficacy of FA-NBs-IR780 upon NIR irradiation *in vivo*. (A) Temperature changes of the tumour surface before and after PTT therapy in the different groups. $*p < 0.05$: compared to the temperature before therapy in the same group. (B) Representative photos of xenograft mice in the different groups with the corresponding times. (C) 2D ultrasound imaging of tumours in the different groups after PTT therapy with the corresponding times. (D) Relative tumour volume (V/V_0) in the different groups changed over time after PTT therapy. $**p < 0.01$: significantly different compared to other groups; $^{\#}p < 0.05$: significantly different compared to FA-NBs group and control group at 15 days; $^{\&}p < 0.05$: significantly different compared to free IR-780 group at 15 days. (E) The body weights of tumour-bearing mice in the different groups changed over time after PTT therapy.

suggesting that local PTT therapy did not produce any significant systemic toxicities.

Antitumor efficacy was further evaluated by immunohistochemical analyses. As shown in Fig. 9, the AI of the NBs-IR780 group was 54.6 ± 3.65%, which was higher than that in the free IR-780 group (34.2 ± 1.87%), the FA-NBs group (23.3 ± 1.52%), and the control group (22.2 ± 2.37%). Consistently, the PI of the NBs-IR780 group was 51.83 ± 2.70%, which was lower than that of the free IR-780 group (65.34 ± 2.20%), the FA-NBs group (76.26 ± 3.42%), and the control group (76.58 ± 3.11%). Strikingly, the number of TUNEL-positive cells (brown) was the highest and the number of PCNA positive cells (brown) was the lowest in the tumours of the FA-NBs-IR780 group, with an AI of 78.6 ± 5.95% and a PI of 25.5 ± 2.27%, which are significantly different compared to the other groups ($p < 0.01$). These results were consistent with the photography and ultrasound results, further confirming that FA-NBs-IR780 exhibited significant therapeutic antitumor effects upon NIR irradiation.

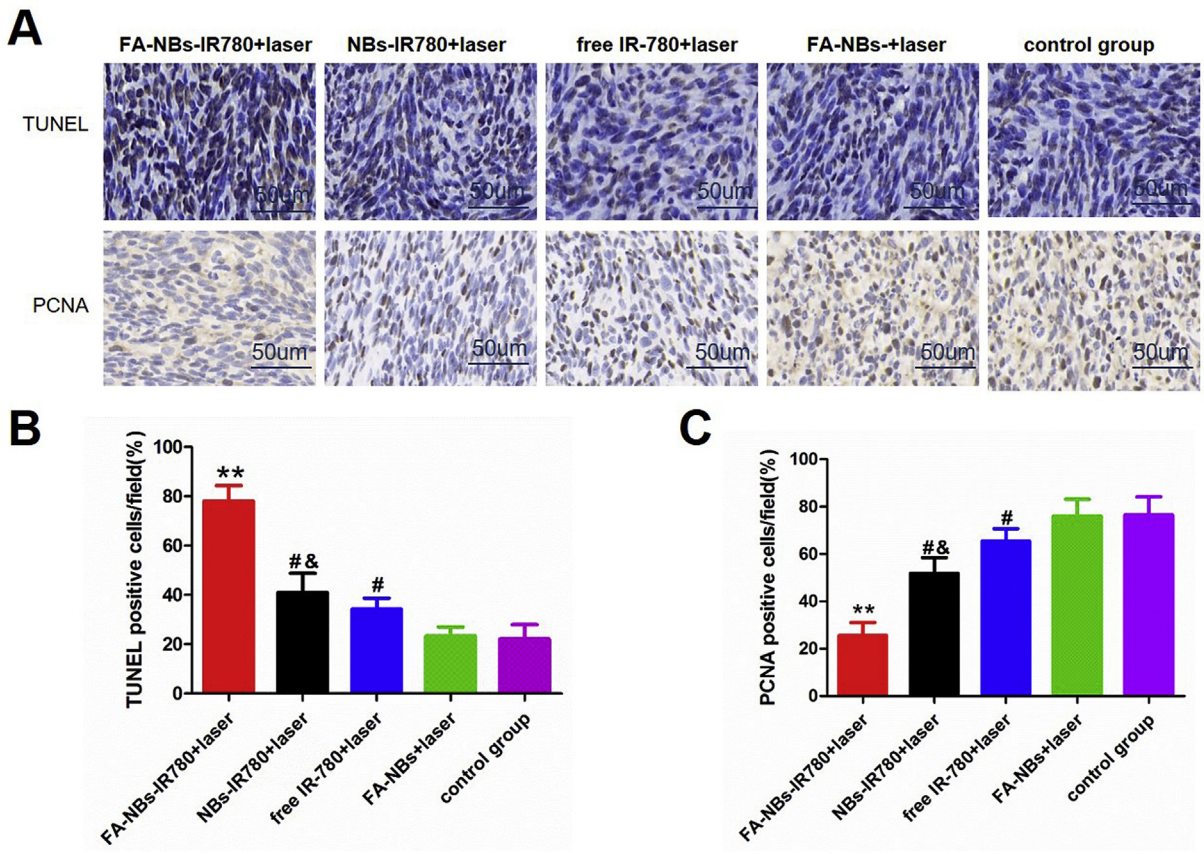

Fig. 9. Immunohistochemical analysis of TUNEL and PCNA in U87 xenograft 3 days after PTT therapy in the different groups. (A) TUNEL staining and PCNA staining in FA-NBs, free IR-780, NBs-IR780, FA-NBs-IR780 and control groups. (B) The cellular apoptosis index via the TUNEL method at 200× magnification. (C) The cellular proliferation index via PCNA at 200× magnification. ** $p < 0.01$: significantly different compared to the NBs-IR780 + laser group; $^{\#}p < 0.05$: significantly different compared to the FA-NBs + laser group and control group; $^{\&}p < 0.05$: significantly different compared to the free IR-780 + laser group.

4. Discussion

Precision oncology has attracted an increasing amount of attention, where early precision diagnosis and targeted therapy are key [28]. Ultrasound provides advantages for cancer diagnosis thanks to its availability and safety. However, its specificity and sensitivity are compromised in traditional UCAs. One solution to this problem is the development of specific UCAs able to target cancers directly [29–31]. Traditional UCAs are produced as MBs with diameters from 1 to 5 μm and are only able to target molecular markers in the vasculature, limiting their application to cancer imaging. However, NBs as nano-sized UCAs have attracted considerable attention in the research sphere [32–34]. As vascular endothelial gap of tumours is approximately 380–780 nm in size, it is important to produce nanobubbles that have diameters smaller than 780 nm [6]. The size of the nanobubbles used in this study were within this range, allowing them to penetrate the endothelial gaps of tumour vessels and circulate into tumour tissues.

To increase the targeting specificity, the nanobubbles were conjugated to various targeting moieties [13,35,36]. Previously, we successfully conjugated HER2 antibodies to NBs, which resulted in an excellent HER2(+) cancer targeting and ultrasound imaging capacity *in vitro* and *in vivo* [13]. Recently, the folate receptor (FR) has attracted attention, since it is generally overexpressed in several human cancers, including lung, breast, ovarian, endometrium, kidney, colon, and brain cancer, but is minimally expressed in normal tissues [14–18]. FR-targeting nanobubbles should therefore provide certain advantages in terms of recognizing different types of cancers. Moreover, in contrast to antibodies, which need to be conjugated to the nanobubble surface via a complex process, folic acid (FA) is a chemical compound that can be easily conjugated to the nanobubbles and other nanoparticles [19,20]. Previous research has proven that FA-modified nanobubbles improve the targeting ability to tumour cells, but it was only used for diagnostic study [37].

It is worth mentioning that NIR dyes with a high fluorescence intensity are considered promising agents for cancer imaging and treatment [38,39]. IR-780 iodide, a representative hydrophobic NIR dye, also has excellent cancer targeting abilities and provides a PTT effect by generating heat upon laser irradiation [40,41]. Despite of these promising advantages, the clinical application of IR-780 iodide has been restricted due to its poor aqueous solubility as well as a result of only a small amount of it being able to reach tumours via the blood. Many efforts have been made to overcome these drawbacks by encapsulating IR-780 iodide in various nano-materials, including polymeric micelles, liposomes, quantum dots, and serum albumin NPs [23,25,40,41]. It is worth noting that, in this study, NBs with liposome membranes were used to encapsulate IR-780 iodide to improve its lipid solubility. Via conjugation with nanobubbles, its water solubility was increased and a higher concentration of IR-780 iodide could be achieved. Moreover, at present, few studies have been carried out using FA and NIR dyes double-conjugated to nanobubbles for the early accurate diagnosis and targeted therapy for cancer.

In this study, we successfully prepared a novel nano-sized multifunctional targeted ultrasound contrast agent, FA-NBs-IR780, with an excellent cancer targeting ability, thanks to the dual targeting capacity provided by FA and IR-780 iodide. So, the NBs accumulate massively at the cancer sites once they pass through the cancer vessels. *Ex vivo* fluorescence imaging further confirmed that FA-NBs-IR780 were mainly metabolized in the lungs, liver, and kidneys. No mice died as a

result of the experiments carried out in this study, indicating the safety of these NBs. All these provide the advantages of this method for accurate cancer molecular-targeted imaging and therapy.

Using ultrasound contrast imaging, we found the imaging intensity of SonoVue MBs was greater than that of NBs at the early stage of perfusion (10 s), mainly due to the micro-size, which results in a high backscatter when in the blood. However, the MBs were unable to pass through the gaps in the tumour vessels, and were therefore attenuated significantly due to the dispersion of interior gas and the clearance function of the body. Several earlier studies have demonstrated that NBs have an ultrasound contrast-enhanced ability [32,33]. In our study, blank NBs were also found to have ultrasound enhanced-imaging abilities, even without a targeting moiety. However, the imaging intensity was low, and the duration time was short. Strikingly, a significantly higher ultrasound enhancement signal was observed in the tumours of FA-NBs-IR780, with a higher peak intensity and a longer duration. This could be due to a number of reasons; firstly, FA-NBs-IR780 have an excellent cancer targeting ability both *in vitro* and *in vivo*. Secondly, NBs possess a porous internal structure with multiple voids, such that, when they are conjugated with targeting ligands, they can be collectively deposited on the surfaces of tissues or cells in a layering effect or can coalescence into large bubbles, creating local acoustic impedance that mismatches and enhances the acoustic contrast for molecular imaging. It is important to note that FA-NBs-IR780 could also be used for NIRF imaging. Referring to previous studies [23], we observed the NIRF imaging of FA-NBs-IR780 at 24 h post-injection. The tumour site of tumour-bearing mice presented brighter fluorescence imaging when treated with FA-NBs-IR780. Although the NBs had indisputable disappeared at this time, the fluorescence efficiency also reflected the amount of IR-780 iodide and the number of NBs. This method not only improved the delivery of IR-780 iodide but also reduced its toxicity. These findings indicate that FA-NBs-IR780 were suitable for accurate early cancer imaging, both as acoustic and optical agents.

Our *in vivo* study showed that IR-780 iodide encapsulated in FA-NBs-IR780 could enhance its heat generation with laser irradiation, resulting in an excellent cancer retardation ability when combined with an NIR laser. Consistently, the local temperature in mice receiving FA-NBs-IR780 was higher than that in mice receiving free IR-780. According to previous studies, a quickly increasing temperature (greater than 45 °C) can lead to irreversible damage [40,42,43], which accounts for the effects of FA-NBs-IR780 on the tumour in this study. These results demonstrated that FA-NBs-IR780 could also be used as photothermal agents for simultaneous PTT therapy. Moreover, since the cancerous region can be imaged and located precisely, only cancer tissues were irradiated during PTT, such that the surrounding normal tissue was minimally hurt. This could greatly improve the therapeutic effects of FA-NBs-IR780 and reduce any systemic side effects associated with this treatment.

In summary, we successfully manufactured novel multi-functional nanobubbles, FA-NBs-IR780, with excellent cancer targeting ability, dual-mode imaging, and striking photothermal responsiveness. The FA-NBs-IR780 were nanosized and stable, and were preferentially enriched in the tumour, allowing for the accurate imaging of cancer by ultrasound and NIRF. IR-780 accumulated at tumour sites by the help of FA-NBs-IR780, resulting in the apoptosis of cancer cells and a reduction of the tumour volume in the targeted region upon NIR radiation. Taken together, our findings indicate that FA-NBs-IR780 is a promising agent for the accurate diagnosis of cancer and for subsequent photothermal therapy.

Conflicts of interest

The authors have declared that no conflict of interest exists.

Acknowledgments

This work was financially supported by the National Natural Science Foundation of China (Grant No. 81671706). The authors thank the Department of Molecular Biology, Fourth Military Medical University, for its technical support and kind provision of equipment.

Appendix A. Supplementary data

Supplementary data to this article can be found online at https://doi.org/10.1016/j.canlet.2019.04.023.

References

[1] R.L. Siegel, K.D. Miller, A. Jemal, Cancer statistics, Ca - Cancer J. Clin. 67 (2017) 7–30 2017.
[2] R. Weissleder, Molecular imaging: exploring the next frontier, Radiology 212 (1999) 609–614.
[3] D.A. Mankoff, M.D. Farwell, A.S. Clark, D.A. Pryma, Making molecular imaging a clinical tool for precision oncology: a review, JAMA Oncol. 3 (2017) 695–701.
[4] M.F. Kircher, J.K. Willmann, Molecular body imaging: MR imaging, CT, and US. Part II. Applications, Radiology 264 (2012) 349–368.
[5] F. Kiessling, S. Fokong, J. Bzyl, W. Lederle, M. Palmowski, T. Lammers, Recent advances in molecular, multimodal and theranostic ultrasound imaging, Adv. Drug Deliv. Rev. 72 (2014) 15–27.
[6] S.K. Hobbs, W.L. Monsky, F. Yuan, W.G. Roberts, L. Griffith, V.P. Torchilin, et al., Regulation of transport pathways in tumor vessels: role of tumor type and microenvironment, Proc. Natl. Acad. Sci. U. S. A. 95 (1998) 4607–4612.
[7] J. Fang, H. Nakamura, H. Maeda, The EPR Effect: unique features of tumor blood vessels for drug delivery, factors involved, and limitations and augmentation of the effect, Adv. Drug Deliv. Rev. 63 (2011) 136–151.
[8] V. Torchilin, Tumor delivery of macromolecular drugs based on the EPR effect, Adv. Drug Deliv. Rev. 63 (2011) 131–135.
[9] H. Maeda, Toward a full understanding of the EPR effect in primary and metastatic cancers as well as issues related to its heterogeneity, Adv. Drug Deliv. Rev. 91 (2015) 3–6.
[10] H. Maeda, T. Sawa, T. Konno, Mechanism of cancer-targeted delivery of macromolecular drugs, including the EPR effect in solid cancer and clinical overview of the prototype polymeric drug SMANCS, J. Control. Release 74 (2001) 47–61.
[11] S.A. Moestue, I.S. Gribbestad, R. Hansen, Intravascular targets for molecular contrast-contrast ultrasound imaging, Int. J. Mol. Sci. 13 (2012) 6679–6697.
[12] W.B. Cai, H.L. Yang, J. Zhang, J.K. Yin, Y.L. Yang, L.J. Yuan, et al., The optimized fabrication of nanobubbles as ultrasound contrast agents for cancer imaging, Sci. Rep. 5 (2015) 13725.
[13] H.L. Yang, W.B. Cai, L. Xu, X.H. Lv, Y.B. Qiao, P. Li, et al., Nanobubble–Affibody: novel ultrasound contrast agents for targeted molecular ultrasound imaging of cancer, Biomaterials 37 (2015) 279–288.
[14] Y.G. Assaraf, C.P. Reddy, J.A. Leamon, The folate receptor as a rational therapeutic target for personalized cancer treatment, Sci. Direct 17 (2014) 89–95.
[15] C. Leamon, P. Low, Folate-mediated targeting: from diagnostics to drug and gene delivery, Drug Discov. Today 6 (2001) 44–51.
[16] K.R. Kalli, A.L. Oberg, G.L. Keeney, T.J. Christianson, P.S. Low, K.L. Knutson, et al., Folate receptor alpha as a cancer target in epithelial ovarian cancer, Gynecol. Oncol. 108 (2008) 619–626.
[17] L.A. Dainty, J.I. Risinger, C. Morrison, G.V.R. Chandramouli, M.A. Bidus, C. Zahn, et al., Overexpression of folate binding protein and mesothelin are associated with uterine serous carcinoma, Gynecol. Oncol. 105 (2007) 563–570.
[18] L.C. Hartmann, G.L. Keeney, W.L. Lingle, T.J.H. Christianson, B. Varghese, D. Hillman, et al., Folate receptor overexpression is associated with poor outcome in breast cancer, Int. J. Cancer 121 (2007) 938–942.
[19] K.S. Li, Y.H. Liu, S.M. Zhang, Y.F. Xu, J.S. Jiang, F.Y. Yin, et al., Folate receptor-targeted ultrasonic PFOB nanoparticles: synthesis, characterization and application in cancer-targeted imaging, Int. J. Mol. Med. 39 (2017) 1505–1515.
[20] B. Bahrami, M. Mohammadnia-Afrouzi, P. Bakhshaei, Y. Yazdani, G. Ghalamfarsa, M. Yousefi, et al., Folate-conjugated nanoparticles as a potent therapeutic approach in targeted cancer therapy, Tumour Biol. 36 (2015) 5727–5742.
[21] X.M. Yi, F.L. Wang, W.J. Qin, X.J. Yang, J.L. Yuan, Near-infrared fluorescent probes in cancer imaging and therapy: an emerging field, Int. J. Nanomed. 9 (2014) 1347–1365.
[22] M. Gao, F.B. Yu, C.J. Lv, J. Choo, L.X. Chen, Fluorescent chemical probes for accurate tumor diagnosis and targeting therapy, Chem. Soc. Rev. 46 (2017) 2237–2271.
[23] C.X. Yue, P. Liu, M.B. Zheng, P.F. Zhao, Y.Q. Wang, Y.F. Ma, et al., IR-780 dye loaded cancer targeting theranostic nanoparticles for NIR imaging and photothermal therapy, Biomaterials 34 (2013) 6853–6861.
[24] C.H. Shi, J.B. Wu, D.F. Pan, Review on Near-infrared heptamethine cyanine dyes as theranostic agents for tumor imaging, targeting, and photodynamic Therapy, J. Biomed. Opt. 21 (2016) 050901.
[25] K.K. Wang, Y.F. Zhang, J. Wang, A. Yuan, M.J. Sun, J.H. Wu, et al., Self-assembled IR780-loaded transferrin nanoparticles as an imaging, targeting and PDT/PTT agent for cancer therapy, Sci. Rep. 6 (2016) 27421.

[26] Gavrieli, Y. Sherman, S.A. Ben-Sasson, Identification of programmed cell death in situ via specific labeling of nuclear DNA fragmentation, J. Cell Biol. 119 (1992) 493–501.
[27] Z. Gao, A.M. Kennedy, D.A. Christensen, N.Y. Rapoport, Drug-loaded nano/microbubbles for combining ultrasonography and targeted chemotherapy, Ultrasonics 48 (2008) 260–270.
[28] E.C. Hayden, Personalized cancer therapy gets closer, Nature 458 (2009) 131–132.
[29] T.T. Luo, J.C. Sun, S.Y. Zhu, J. He, L. Hao, L.L. Xiao, et al., Ultrasound-mediated destruction of oxygen and paclitaxel loaded dual-targeting microbubbles for intraperitoneal treatment of ovarian cancer xenografts, Cancer Lett. 391 (2017) 1–11.
[30] T. Zhou, W.B. Cai, H.L. Yang, H.Z. Zhang, M.H. Hao, L.J. Yuan, et al., Annexin V conjugated nanobubbles: a novel ultrasound contrast agent for in vivo assessment of the apoptotic response in cancer therapy, J. Control. Release 276 (2018) 113–124.
[31] M.M. Meng, J. Gao, C.C. Wu, X. Zhou, X.F. Zang, X.C. Lin, et al., Doxorubicin nanobubble for combining ultrasonography and targeted chemotherapy of rabbit with VX2 liver tumor, Tumour Biol. 37 (2016) 8673–8680.
[32] J. Ma, C.S. Xu, F. Gao, M. Chen, F. Li, L.F. Du, Diagnostic and therapeutic research on ultrasound microbubble/nanobubble contrast agents (Review), Mol. Med. Rep. 12 (2015) 4022–4028.
[33] T.H. Yin, P. Wang, R.Q. Zheng, B.W. Zheng, D. Cheng, X.L. Zhang, et al., Nanobubbles for contrast ultrasound imaging of tumors, Int. J. Nanomed. 7 (2012) 895–904.
[34] R. Cavalli, M. Soster, M. Argenziano, Nanobubbles: a promising efficient tool for therapeutic delivery, Ther. Deliv. 7 (2016) 117–138.
[35] Q.C. Jiang, S.Y. Hao, X.Y. Xiao, J.Y. Yao, B. Ou, Z.Z. Zhao, et al., Production and characterization of a novel long-acting herceptin-targeted nanobubble contrast agent specific for Her-2-positive breast cancers, Breast Canc. 23 (2016) 445–455.
[36] Y. Gao, C. Hernandez, H.X. Yuan, J. Lilly, P. Kota, H.Y. Zhou, et al., Ultrasound molecular imaging of ovarian cancer with CA-125 targeted nanobubble contrast agents, Nanomedicine 13 (2017) 2159–2168.
[37] S.J. Duan, L. Guo, D. D Shi, M.M. Shang, D. Meng, J. Li, Development of a novel folate-modified nanobubbles with improved targeting ability to tumor cells, Ultrason. Sonochem. 37 (2017) 235–243.
[38] A. Yuan, J. h. Wu, X.L. Tang, L.L. Zhao, F. Xu, Y.Q. Hu, Application of near-infrared dyes for tumor imaging, photothermal, and photodynamic therapies, J. Pharm. Sci. 102 (2013) 6–28.
[39] K. Sato, T. Nagaya, M. Mitsunaga, P.L. Choyke, H. Kobayashi, Near infrared photoimmunotherapy for lung metastases, Cancer Lett. 365 (2015) 112–121.
[40] C.X. Jiang, H. Cheng, A. Yuan, X.L. Tang, J.H. Wu, Y.Q. Hu, Hydrophobic IR780 encapsulated in biodegradable human serum albumin nanoparticles for photothermal and photodynamic therapy, Acta Biomater. 14 (2015) 61–69.
[41] S.H. Li, S.X. Zhou, Y.C. Li, X.H. Li, J. Zhu, L.Z. Fan, et al., Exceptionally high payload of the IR780 iodide on folic acid-functionalized graphene quantum dots for targeted photothermal therapy, ACS Appl. Mater. Interfaces 9 (2017) 22332–22341.
[42] Y.N. Yu, Z.P. Zhang, Y. Wang, H. Zhu, F.Z. Li, Y.Y. Shen, et al., A new NIR-triggered doxorubicin and photosensitizer indocyanine green co-delivery system for contrast multidrug resistant cancer treatment through simultaneous chemo/photothermal/photodynamic therapy, Acta Biomater. 59 (2017) 170–180.
[43] F. Guo, M. Yu, J.P. Wang, F.P. Tan, N. Li, Smart IR780 theranostic nanocarrier for tumor-specific therapy: hyperthermia-mediated bubble-generating and folate-targeted liposomes, ACS Appl. Mater. Interfaces 7 (2015) 20556–20567.